Journal of Materials Chemistry A

Accepted Manuscript

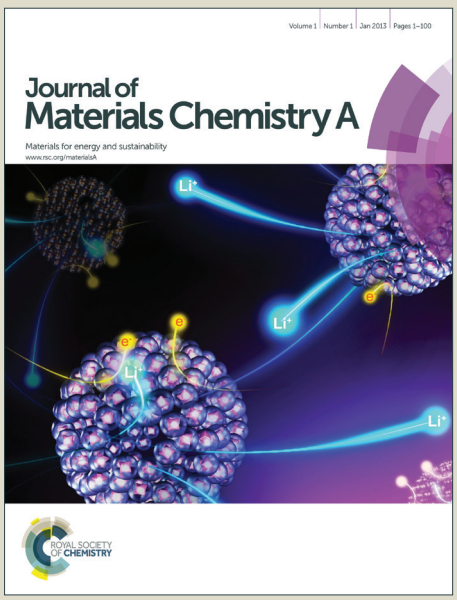

ROYAL SOCIETY OF CHEMISTRY

www.rsc.org/materialsA

Journal of Materials Chemistry A
CREATED USING THE RSC LaTeX PCCP ARTICLE TEMPLATE – SEE www.rsc.org/electronicfiles FOR DETAILS
ARTICLE TYPE www. rsc.org/xxxxxx | XXXXXXXX

Lithium peroxide precursor on the α-MnO_2 (100) surface.

Yanier Crespo,*[a] and Nicola Seriani [a]

DOI: 10.1039/b000000x

α-MnO_2 is an active electrocatalyst for the cathode of lithium-air batteries, where the main reaction is the reversible formation of lithium peroxide. In this work we study adsorption of lithium and oxygen on the low-energy (100) surface by atomistic simulations based on density functional theory, in order to understand the first steps of lithium peroxide formation. Oxygen prefers to adsorb in molecular form both in presence and in absence of co-adsorbed lithium. This represents a marked difference with respect to other manganese oxides, where oxygen dissociation takes place, and we argue that this might be of advantage in the formation and dissolution of lithium peroxide. By studying the formation energies of Li_2O_2-like species at the surface we have identified the most probable precursor for the formation of Li_2O_2 nanoparticles on this surface. The possible consequences of these findings for the functionality of the battery are discussed.

1 Introduction

Renewable energy sources, like solar and wind, suffer from the limitation of being available intermittently. This increases the importance of energy storage and as a consequence a large effort is devoted to the development of new devices for this purpose. One of the main issues that need to be resolved is that of increasing the energy density of the devices. To reach this goal, a promising candidate system is the Li-air battery, that has a theoretical gravimetric energy density comparable to that of gasoline[1–7]. However, experimental studies done in practical prototypes of Li-air batteries have shown that they suffer from high recharging overpotentials and poor cyclability. In order to be able to bring these problems under control, it is essential to understand the main process taking place at the cathode, namely the reversible formation of lithium peroxide.

To enhance the performance of Li-air batteries, catalysts have been introduced in the oxygen cathode; among them, α-MnO_2 is the most promising[8–11], increasing the capacity and the cyclability of the battery. A recent study on different Li-air electrocatalysts[8] has shown that α-MnO_2 nanowires give the highest charge storage capacity and cyclability among all the catalysts studied, and are superior to other MnO_2 polymorphs, like γ-MnO2, β-MnO2 and λ-MnO2. Also Trahey and co-workers studied the effect of α-MnO_2/ramsdellite-MnO_2 when used as an electrode/electrocatalyst for Li-air cells[12]. They found that this electrode provided an exceptionally high reversible capacity during the early cycles, contrary to the cell where this catalyst was not present. In addition, the presence of α-MnO_2/ramsdellite-MnO_2 reduces significantly the polarization during the first couple of cycles.

It seems thus that α-MnO_2 has a quite unique eletrocatalytic properties for the reaction of lithium and oxygen. Indeed, in other contexts it has been shown that it is an active catalyst for oxygen reduction reactions, for the oxidation of ammonia with NO[13], and that of methane[14] in presence of visible light, or water[15]. In order to understand the properties at the origin of the high activity of α-MnO_2, several theoretical studies have appeared in the last years[12,16–21]. In particular, great attention has been devoted to the insertion of lithium, lithium oxide and impurities into the channels of this compound.

Using density functional theory (DFT) with the Hubbard correction (DFT+U), Cockayne *et al.*[17] found that the insertion of potassium, water, OH^- and H_3O^+ occurs easily and stabilize the compound. By the same method, Ling *et al.*[16] have investigated the insertion of Li ions and Li oxide, and found that the insertion of lithium oxide Li_2O into the channels of bulk α-MnO_2 is reversible, while the insertion of high concentrations of lithium ions lead to irreversible structural modifications[16]. Later Tompsett *et al.*[18] confirmed the the differences between insertion of lithium and insertion of lithium oxide, found that Li_2O incorporation leads to a metallic character of the compound, which is of advantage for battery operation[18]. Trahey *et al.*[12] investigated the formation of lithium oxides in the channels of bulk α-MnO_2 and concluded that Li_2O insertion and lithiation might increase the activity of α-MnO_2 as an electrocatalyst, by donating electrons to manganese and lead to the formation of Mn^{+3} ions. Indeed, charge donation by impurities in the channels have been shown to change the electronic and magnetic properties of α-MnO_2, even leading to the formation of spin glasses[19,22,23].

Still, the reaction mechanisms of lithium peroxide formation and decomposition in presence of α-MnO_2 and the role of this oxide in side-reactions and parasitic reactions, like the formation of lithium carbonate Li_2CO_3, are still subject to investigation[4,12,24]. It is however established that lithium peroxide does not form in the channels of α-MnO_2, but outside of the manganese oxide[25]. It is therefore probable that the rel-

* *E-mail: ycrespo@ictp.it*
[a] *The Abdus Salam ICTP, Strada Costiera 11, I-34151 Trieste, Italy*

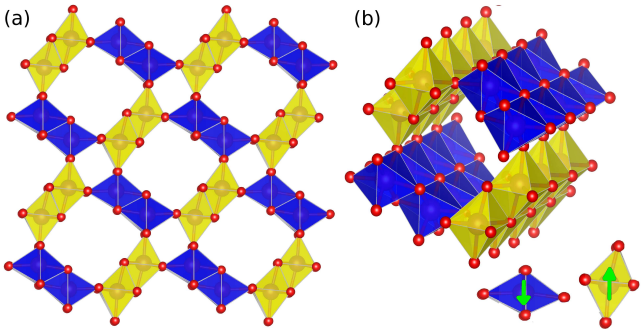

Fig. 1 (Color online) Different views of the hollandite structure for the case of α-MnO_2 compound [22,23] (a) the xz plane containing the Mn atoms and the two types of oxygen atoms the one with sp^2 hybridization ($O(sp^2)$) and those with sp^3 hybridization ($O(sp^3)$) (b) panoramic view of the channel where the two types of oxygen hybridization can be better observed. The small red balls represent oxygen atoms, the large violet balls represent manganese atoms.

evant reactions should take place at the surface of α-MnO_2. This fact might also be related to the observation that the behaviour of α-MnO_2 nanowires is superior to that of bulk α-MnO_2[8]. Nevertheless, the surfaces have been poorly characterized. We are only aware of a recently study employing density functional theory (DFT) to investigate magnetism and OH^- adsorption on α-$MnO_2(110)$[21], but lithium adsorption and reaction with oxygen was not investigated. These reactions have only been investigated on the (110) surface of the different compound β-MnO_2[26], where oxygen was found to adsorb dissociatively.

To systematically understand the chemical processes occurring at the Li-air cathode in the presence of the α-MnO_2 nanowires catalyst in this paper we perform an *ab-initio* study of the adsorption properties of the low-index surface (100), by DFT+*U*. We show that this surface has a low surface energy, comparable to that of (110) and lower than that of (001). Then adsorption of oxygen and lithium is investigated on this surface. Oxygen dissociation is disfavored both in absence and in presence of lithium. The formation energy of a Li-O-O-Li unit with a geometry similar to that of bulk Li_2O_2 is lower than that of bulk Li_2O_2. We discuss how the above results might be at the origin of the high capacity and cyclability shown by this material.

The rest of this article is organized as follows: we present the computational methods used for this calculations in Sec.2. Then we study the surface energy of three stoichiometric surfaces, the oxygen adsorption and the formation of Li-O-Li and Li-O-O-Li species on the (100) surface and we discuss the implications for Li-air batteries in Sec.3. Finally conclusions are given in Sec.4.

2 Computational methods

All calculations are based on density functional theory (DFT) with the Hubbard correction (DFT+*U*) to properly describe the 3d shell of manganese. The performance of post-DFT methods such as DFT+*U* or hybrid functionals on different Mn oxides was carefully investigated in the literature[20,27]. In particular, for α-MnO_2 it was shown[20] that DFT+*U* with $U > 2.0$ eV and hybrid functionals do not reproduce the antiferromagnetic ground state observed in the experiments[28]. On the contrary, for smaller values of *U* an antiferromagnetic ground state is obtained. Therefore we have performed spin-polarized, *ab-initio* calculations using the DFT+*U* technique [29,30] with the Quantum-Espresso package[31], with *U=1.6* eV, as suggested in Ref. [20]. The DFT+*U* calculations were carried out in the simplified version of Dudarev *et al.*[32] as implemented by Cococcioni et al.[33]. An exchange-correlation functional in the generalized-gradient approximation was employed in the version of Perdew, Burke and Ernzerhof[34], together with Vanderbilt ultrasoft pseudopotentials[35].

For the wavefunctions and the charge density, energy cutoffs of 30 Ry and 300 Ry have been respectively employed. A mesh of $(1\times6\times1)$ k-points, generated with the method of Monkhorst and Pack [36], was sufficient for the integration in the first Brillouin zone of the elementary cell used for the study of the bulk structural properties[20]. Surface calculations were performed on slabs with symmetrically equivalent surfaces, stoichiometric composition and thickness between 15 and 19 Å, depending on the surface plane. For the (100) surface we employed a thickness of 17.8 Å, corresponding to 23 layers counted as in Ref.[21]. A vacuum thickness of approximately 10 Å was sufficient to obtain convergence of the surface energy. Atomic positions were relaxed until forces were smaller than 10^{-3} a.u. In the slab calculations, all atomic position were relaxed. In the middle of the slab, the Mn-O distances changed at most by 0.02 Å during relaxation, thereby retaining their bulk values. As initial magnetic order we imposed the antiferromagnetic configuration reported to be the ground state in previous studies[17,20]. The order did not change during the calculation. Surface energies (γ) are calculated as

$$\gamma = \frac{E_{slab} - nE_{bulk}}{2A}, \quad (1)$$

where E_{slab} is the total energy of the slab containing *n* formula units, E_{bulk} is the total energy per formula unit of bulk α-MnO_2 and *A* is the surface area of one of the two symmetric surfaces of the slab. In all cases adsorption energies where obtained using as a reference the DFT energies for isolated molecular oxygen and for bulk body centered cubic lithium. The binding energy of the O_2 molecule is affected by an overbinding error in DFT. To estimate this error, we have followed the approach of Ref.[26] and calculated the formation energies of bulk GeO_2, TiO_2 and ZrO_2. It results that

DFT with our parameters overestimates the oxygen binding energy by 0.43 eV/O atom. This means that our values need to be shifted down accordingly but our conclusions are robust against this error.

3 Results and discussion

3.1 Stoichiometric surfaces energies

We have investigated the energetics of three low-index surfaces, namely (100) (equivalent to (010)), (001) and (110). Cutting the crystal along the (100) and (110) directions leads to the formation of 5-coordinated Mn (5c-Mn) ions and two-coordinated oxygen atoms (see Figs.2 (a) and (b)). Other terminations of these surfaces would lead to the creation of larger numbers of dangling bonds, therefore they have not been considered in this work. On the contrary, cutting along the (001) direction requires either the creation of four-coordinated Mn atoms or singly-coordinated oxygen atoms, with substantially higher energy costs. This qualitative picture is confirmed by the calculations (Table 1), with the surface energies ordered as follows: $\gamma \approx 0.68$ J/m^2 for the (100) surface in both DFT and DFT+U. Almost the same energy $\gamma = 0.70$ J/m^2 is obtained for the (110) surface by using DFT+U, in agreement with the value obtained ($\gamma = 0.77$ J/m^2) in a recent DFT study[21]. A larger $\gamma = 1.41$-1.50 (DFT-DFT+U) J/m^2 is found for the (001) surface. These results are qualitatively in agreement with the observation that the two surfaces (100) and (110) are the most commonly found in α-MnO_2 nanowires[37–42].

To have a more quantitative comparison with the experiments, one can consider the shape of nanostructures. Wulff's theorem states that, in the shape that minimizes the energy of a particle, each facet has distance form the center of the particle which is proportional to its surface energy[43]. Therefore it is possible to build the equilibrium shape by using the surface energies of the different facets[43–45]. In the present case, the (100) and (110) have similar surface energies, and the calculated ratio of the (100) and the (001) surface energies is $\sim$2.1; this should correspond to the aspect ratio of particles at equilibrium. In most experiments on nanostructured α-MnO_2 only (100) and (110) facets were observed[37–42] but also the (001) was seen in experiment[28]. However, the aspect ratio observed in α-MnO_2 nanostructures is larger than the calculated one: for example in Ref.[46], rods with a diameter of 18 nm and lengths between 0.2 and 1.0 μm were produced; in Ref.[47], wires with diameters of 20-50 nm and lengths of 2-8 μm were synthesized; in Ref.[37], nanorods with diameters of 40-80 nm and lengths of 300-800 nm were observed. So, in all these experiments, the nanostructures are more elongated than Wulff construction suggests. This discrepancy could be explained by two effects: it could be due to the adsorption of other chemical compounds not considered in this work, which would modify the surface free energies of the facets and therefore the aspect ratio (thermodynamic effect); or it could be due to the preparation conditions employed for the production of the nanostructures to produce a non-equilibrium shape (kinetic effect). Understanding the origin of these discrepancies requires further investigations that go beyond the scope of this paper.

Table 1 Surface energies in J/m^2 for α-MnO_2 for three types of surfaces: (100), (110) and (001). Two calculations are shown DFT and DFT+U (U = 1.6 eV):

Surface Plane	(100)	(110)	(001)
DFT	0.67	0.64	1.41
DFT+U (1.6)	0.68	0.70	1.50

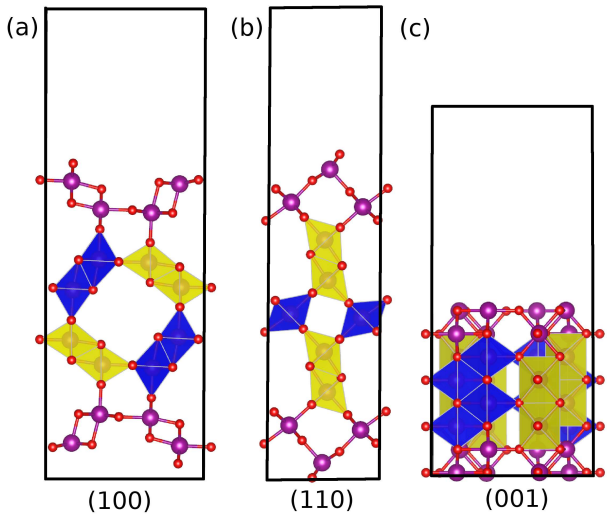

Fig. 2 Supercells containing the simulated α-MnO_2 surfaces slabs for three low Miller indexes (a) (100) (b) (110) (c) (001). The small red balls represent oxygen atoms, the large violet balls represent manganese atoms.

We have shown that the (100) is indeed present in nanostructures at equilibrium. Now on this surface we consider processes relevant for Li-air batteries, namely the adsorption of oxygen and lithium.

3.2 Oxygen adsorption at the α-MnO_2 (100) surface

Atomic oxygen and molecular oxygen adsorption on α-MnO_2(100) have been considered. The three stable configurations we found are shown in Fig.3. Before adsorption, at the surface there are 5-coordinated Mn ions. We have considered (a) a dissociatively adsorbed oxygen called "Atomic", (b) a molecularly oxygen adsorbed in the top of one of the 5c-

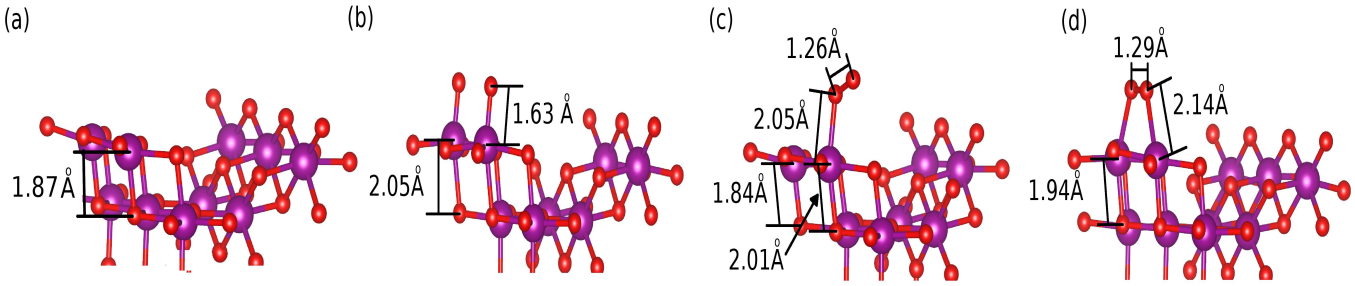

Fig. 3 Oxygen adsorption sites at the α-MnO_2(100) surface: (a) stoichiometric surface (b) atomically adsorbed oxygen; (c) Molecular (on top) adsorption (c) Molecular (bridge) adsorption. The small red balls represent oxygen atoms, the large violet balls represent manganese atoms.

Mn ions called "Molecular Top" and (c) molecular oxygen adsorbed in a bridge position between two 5c-Mn called "Molecular Bridge". We considered also a configuration where a dissociatively adsorbed oxygen is in a bridge position between the two 5c-Mn ions, but this relaxes into one of the stable configurations. Since there are only two adsorption sites in the simulation cells, given by the two 5-coordinated Mn atoms, adsorption of one O atom corresponds to a coverage of 1/2 monolayer (ML). Since molecular oxygen also adsorbs on the same site, a single adsorbed molecule also corresponds to 1/2 ML. The values of the adsorption energies of oxygen for the stable configurations are shown in Table 2. The energy gain for molecular adsorption is 0.20-0.56 eV/O_2 molecule, depending on the functional and the position. The most stable configuration is the "Molecular Bridge" configuration, with an adsorption energy of 0.56 eV/O_2 molecule in DFT and 0.24 eV/O_2 molecule in DFT+U. Dissociation of the oxygen molecule is energetically unfavorable on this surface by ≈0.2-1.55 eV/O_2 molecule with respect to the configurations with molecular adsorption. It should be noticed that our cell has lateral dimensions of 9.92 Å× 5.80 Å, i.e. these adsorption energies refer to a high-density case where adsorbate-adsorbate interaction is not negligible. This is the relevant case when studying the nucleation of lithium peroxide on the surface, because we assume a high density of adsorbates must be present at the surface before nucleation can start.

Table 2 Adsorption energies of oxygen (in eV/O_2) for α-MnO_2 on (100) surface: Three configurations are shown: a dissociatively adsorbed oxygen called "Atomic" and two molecularly adsorbed oxygen called "Molecular Top" and "Molecular Bridge" (see also Figs. 2 and 3).

O_2 Adsorption (100)	Atomic	Molecular Bridge	Molecular Top
DFT	0.20	−0.56	−0.38
DFT+U (1.6)	1.55	−0.24	−0.20

The O-O distance in the molecule adsorbed on (100) is just slightly higher than in the isolated oxygen molecule, namely 1.26 Å for "Molecular Top" and 1.29 Å for "Molecular Bridge". It is instructive to speculate about the possible consequences of this adsorption behaviour for the catalytic activity of α-MnO_2 for oxygen evolution reaction (OER) and oxygen reduction reaction (ORR), in the context of Li-air batteries. It has been suggested that lithium peroxide formation takes place through a mechanism involving the formation of surface adsorbed oxygen ions[48]. In fact, even in the final product lithium peroxide (Li_2O_2), oxygen is present as O_2^{2-} ions[49,50]. We think that the fact that oxygen adsorption is molecular could be crucial for the effectiveness of this material as we will discuss in Sec.3.5. If one plots the catalytic activities of catalysts as a function of their adsorption energies for reactants, usually one obtains a volcano curve[51], *i.e.* the catalytic activity is maximal at some intermediate adsorption energies. However, volcano curves have been established for oxygen evolution reactions only for the case where adsorbed atomic oxygen is a reaction intermediate[52,53], while a comparable study for reactions where oxygen appears only in molecular form is still lacking.

To further investigate the role of α-MnO_2 as catalyst, we notice that it has been recently proposed that highly active transition metal oxide catalysts for the oxygen evolution reaction are characterized by an occupation around 1 of the relevant e_g state of the surface cations[54,55]. They proposed that the occupation of the outward-pointing e_g states of surface cations (5c-Mn) is an activity descriptor for the oxygen evolution reaction of perovskites. It is not established whether this descriptor works also for other transition metal oxides with cations in octahedral coordination. It is thus interesting to calculate the occupation of the 3d states for our compound, which is known to be a good catalyst for this reaction. In fact, for the (100) surface the relevant e_g state (the d_{z^2} state) has an occupation of 0.94 in DFT and 0.95 in DFT+U, as calculated by

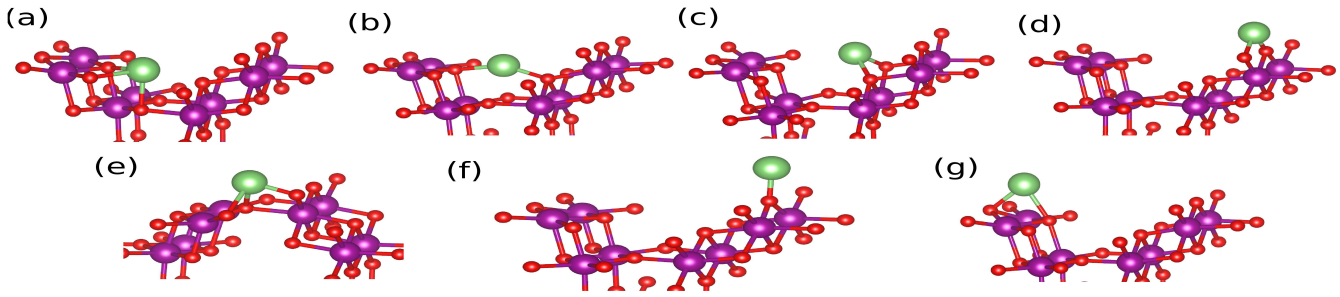

Fig. 4 Li adatom adsorption sites at the (100) surface of α-MnO_2. Seven stable positions where found. The small red balls represent oxygen atoms; the large violet balls represent manganese atoms; the green atoms represent lithium atoms.

the Löwdin method[56]. Thus the very active catalyst α-MnO_2 also fulfills the criterion of having an occupation ~ 1 for the e_g state of the surface 5c-Mn where oxygen can be adsorbed.

As can be seen from Table 2 the two methods used here yield the same trend in the adsorption energies of oxygen at the (100) surface and the relative difference between them is of the order of 0.2 eV/O_2. For this reason, taking into account also that the adsorption energies of Li adatom and the formation energies of Li_2O_2 molecule at the (100) surface of α-MnO_2 are of the order of $1-3$ eV, we have decided to use only the DFT+U method with $U = 1.6$ eV in the following, as no additional information will be obtained with the standard DFT approximation.

3.3 Lithium adsorption at the α-MnO_2 (100) surface

As a second step, lithium adsorption on (100) has been investigated. The adsorption energies for the stable adsorption sites are shown in Table 3. We have found 7 stable positions on the (100) surface of α-MnO_2 and they are shown in Fig.4. Therefore, a single adsorbed Li in the simulation cell corresponds to 1/7 ML = 0.14 ML. Li is strongly adsorbed on this surface with values that go from -1.40 to -3.35 eV/Li. The strongest adsorption occurs in sites with high oxygen coordination that are far from the 5c-Mn ions, meaning that the Li adatom prefers to get adsorbed inside the depression present at this particular surface, created by cutting a channel of the crystal during surface formation (sites (a), (b) and (c)). The adsorption energies in these sites are similar to those obtained inside the channel in the bulk, at the 8h Wyckoff position (~ -3.3 eV/Li)[16,18]. That bulk site corresponds to our (a) site, which gives the strongest adsorption at the surface. When the Li adatom is adsorbed in positions near the 5c-Mn ions ((e) and (g)) or with low oxygen coordination ((f)), the adsorption is weaker. This change is probably due to the electrostatic interaction between the Li and the Mn ions, and the small number of nearest-neighbour oxygen ions. We have estimated the upper limit of the (100) surface capacity, considering a nanoparticle with (100) and (001) surfaces only and the aspect ratio of 2.1 given by the Wulff construction[43] (see Sec. 3.1). From this one can calculate the total (100) surface area ($33.6\, d^2$) and volume ($16.8\, d^3$) of the nanoparticle in dependence of the distance d of a (100) facet from the center of the nanoparticle. The total charge present at (100) surfaces is their total area divided by the area of the surface cell (57.54 Å) and multiplied by 7 times the charge of the electron. The total mass is the volume divided by the density (2.47 a.u./Å^3). The capacity C is then the charge divided by the mass: C = 2639.82 mAh/(d/Å)/g. If we take d = 100 Å, similar to what is observed in the experiments, then we get: C = 26 mAh/g. Thus these seven adsorption sites for lithium correspond to a surface capacity of $\sim$30 mAh/g. Of course, a simultaneous occupation of all seven sites would result in a high Li-Li repulsion. This value therefore represents a theoretical upper limit for the surface capacity.

All the adsorption energies inside the semi-channel at the surface are near in energy, differing from each other by $\sim$60 meV at most. This row of sites with similar energies along

Table 3 Adsorption energies of a Li adatom (in eV/Li atom) on the (100) surface of α-MnO_2 and distances to the nearest surface oxygens (Li-O) given in Å , calculated with DFT+U: seven stable positions were found and the labels (a),(b),...,(g) correspond to the configurations shown in Fig.4.

Adsorption site	Energy (eV/Li)	Li-O d (Å)
(a)	-3.35	1.97, 2.16×2, 2.5×2
(b)	-3.29	1.86, 1.89, 2.37, 2.45
(c)	-3.22	1.99×2, 2.52, 3.1×2
(d)	-3.30	1.85×2
(e)	-2.87	1.78,2.12×2
(f)	-2.67	1.70
(g)	-1.40	1.96,2.14

the channel direction might facilitate the migration of lithium ions along the semi-channel. On the contrary, migration of the atom in the direction perpendicular to the channel is clearly disfavoured, because the lithium has then to go through sites which lie at least 1.3 eV higher in energy.

To study how much charge is transferred from the Li adatom to the surface and where this charge goes, we have performed a Bader analysis[57] and a Löwdin analysis[56] of the charge distribution in the system. We have calculated effective charges and atomic magnetic moments. To obtain the total charge of the atoms, the charge of the core electrons has been added to the charge of the valence electrons calculated by the code. In the Bader analysis, the atomic magnetic moments have been calculated as difference between the Bader charges for the up and down spins. As shown below, the absolute values of the effective charges are quite different between the two methods, but the magnetic moments and the trends in effective charges yield a consistent picture, e.g. over the fate of the charge donated by adsorbed lithium. Depending on the adsorption site the amount of charge donated to the surface is between $+0.90|e|$ and $+0.93|e|$ for Bader and between $+0.30|e|$ and $+0.60|e|$ for Löwdin. It is well known that effective charges are usually different from formal oxidation states[57,58]. Since oxygen formally has an oxidation number of -2, the additional charge is expected to go to the manganese cations. In fact, the variations of the effective charges of the Mn atoms upon Li adsorption are rather small (hundredths of an electronic charge). Roughly half of the charge donated by Li goes on the O atoms surrounding it. A clearer message is brought by the magnetic moments of the ions. Indeed, it was noticed before that considering the change in magnetic moments gives a better indication about cation reduction than the effective charges[26,59]. The main change in magnetic moment is located on the 5c-Mn cation, that is farther to the Li adsorption site. The variations of the magnetic moments $\Delta\mu$ are reported in Table 4. Li adsorption produces changes of the magnetic moments between $\Delta\mu = 0.33\mu_B$ and $\Delta\mu = 0.54\mu_B$ in this 5c-Mn cation, while the changes in all the other Mn cations are $\Delta\mu \leq 0.1\mu_B$. This is consistently shown by both Bader and Löwdin analysis. To test whether other locations could be possible for the large magnetic moment, we have employed the method proposed in Ref.[26]. This method is used to try to localized the magnetic moment at other Mn ions. In particular, we tested the hypothesis that the magnetic moment could be localized on a 6c-Mn ion closer to the Li adsorption site. Electrostatic considerations might lead to think that this could be a good site for the additional charge. As a result of this procedure, we obtain that the localization of the charge in a 6c-Mn is not stable and it always prefers to go to the 5c-Mn. Similar results were observed in the case of the β-MnO_2 polymorph[26].

Table 4 Total charge donated to the surface (Li^+), change on the magnetic moment $\Delta\mu$ of the 5-coordinated Mn atom (5c-Mn) and the change in distance Δd to the oxygen atom below the surface plane (5c-Mn)-O, calculated with DFT+U. The labels (a),(b),..,(g) correspond to the configurations shown in Fig.4.

Adsorption site	$\Delta\mu$ (Bader) (μ_B)	$\Delta\mu$ (Löwdin) (μ_B)	(5c-Mn)-O Δd (Å)
(a)	-0.49	-0.48	0.24
(b)	-0.45	-0.45	0.24
(c)	-0.45	-0.49	0.24
(d)	-0.41	-0.44	0.2
(e)	-0.50	-0.54	0.26
(f)	-0.38	-0.4	0.17
(g)	-0.33	-0.34	0.1

As a consequence of the change in the spin polarization of the 5c-Mn cation, the distances of the truncated octahedra with the five oxygen atoms increase; the largest change is produced in the oxygen that is below the plane formed by the other 4 oxygen atoms and the 5c-Mn cation. This change in the distance (Δd) is between 0.1 and 0.24 Å (see Table 4), and is strictly correlated to the change in magnetic moment, i.e. the longer the change in spin polarization the longer the change of this distance.

3.4 Surface Li_2O_2 precursor:

Experimentally it have been established that in a *aprotic* electrolyte the fundamental cathode discharge product is Li_2O_2[4,24]. Still, Li_2O has very similar energetics[50] and might have negative consequences for the reversibility, since Li_2O formation needs O_2 dissociation, while Li_2O_2 formation does not. In order to shed light over the reaction paths that lead to the formation of Li_2O_2 or Li_2O, we have investigated the first steps of the reaction of lithium with oxygen on α-MnO_2 (100).

Among all possible configurations considered in the previous subsections for the separate adsorption of oxygen and lithium, we took the low-energy structures to build configurations for the co-adsorption of two Li atoms and two oxygen atoms, with both molecular and dissociated oxygen, to investigate the formation of Li-O-O-Li and Li-O-Li species. In the co-adsorption case two Li and two O atoms cover a substantial portion of the surface. It is unclear to which coverage this case corresponds, because to calculate the coverage it would be necessary to know how many Li's and O's are needed to form a full monolayer of adsorbates. This however depends on the atomic structure of such a monolayer, which is not known. We considered configurations where oxygen is adsorbed on Li or on 5c-Mn. We also considered configurations where Li is adsorbed on top of a previously adsorbed oxygen

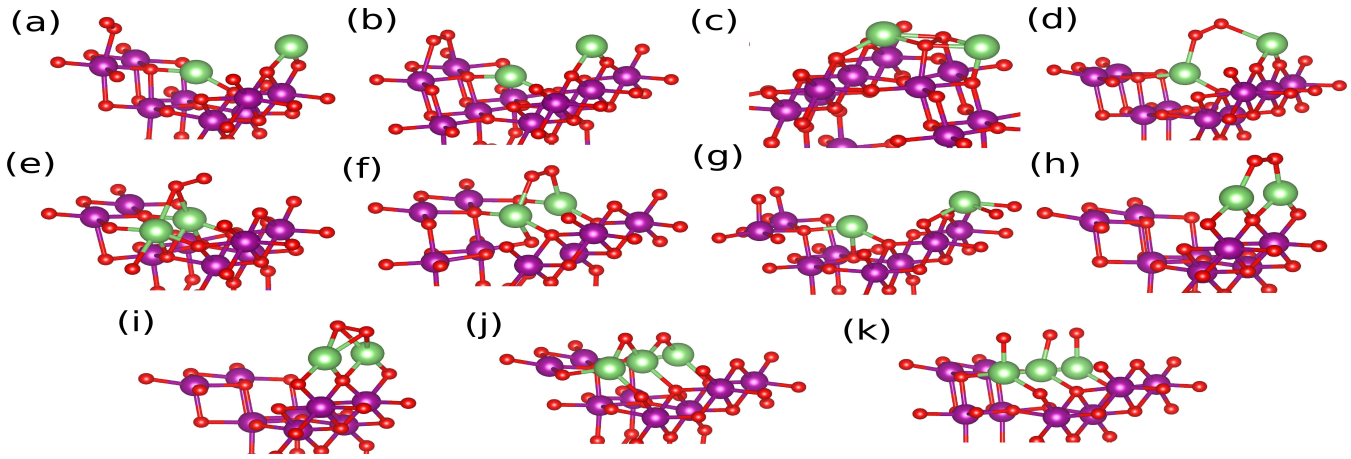

Fig. 5 Selected Li_2O_2 configurations at the (100) surface of α-MnO_2. The small red balls represent oxygen atoms; the large violet balls represent manganese atoms; the green atoms represent lithium atoms.

molecule. The resulting low-energy structures are shown in Fig. 5. Adding the two Li atoms to the surface reduces both 5c-Mn cations present at the surface in the simulation cell, as confirmed by inspection of the magnetic moments.

The formation energies for the configurations shown in Fig. 5 are given in Table 5, as well as the oxygen adsorption energies obtained for both cases of molecular and atomic adsorption. α-MnO_2 (100) offers several sites where Li-O-O-Li species can be formed, with a relatively exothermic adsorption ($E_{ads} \leq -2.86$ eV/Li). On the contrary, Li-O-Li species are completely disfavored, with adsorption energies lying at least 1.6 eV/Li above the formation energies of the Li-O-O-Li species. Once lithium is adsorbed, molecular adsorption of oxygen is always favorable, while dissociative adsorption is endothermic (E_{ads} = 0.26 eV for case (g) and $\geq$ 3.58 eV for cases (j) and (k)). Lithium adsorption on pre-adsorbed oxygen is disfavored with respect to adsorption of oxygen on pre-adsorbed lithium, with adsorption energies in the range $-2.0 \rightarrow -2.56$ eV/Li/O_2.

Table 5 Adsorption energies of Li_2O_2 (in eV/Li/O_2 atom) on the (100) surface of α-MnO_2 and oxygen adsorption on the lithiated surface, calculated with DFT+U. Data is shown for the selected configurations (a),(b),....,(k) of Fig. 5.

Adsorption site	Energy (eV/Li/O_2)	Oxygen adsorption (eV/O_2)
(a)	−3.29	−0.33
(b)	−3.24	−0.23
(c)	−3.23	−0.18
(d)	−3.23	−0.22
(e)	−3.02	−0.15
(f)	−3.00	−0.10
(g)	−3.00	+0.26
(h)	−2.97	−0.92
(i)	−2.87	−0.72
(j)	−1.15	+3.58
(k)	−1.06	+3.76

The most stable configurations (Fig. 5 (a) and (b)) have the oxygen molecule adsorbed on top of the 5c-Mn and the two Li atoms adsorbed to the α-MnO_2, not to the adsorbed oxygen. Still, there is also a configuration with a Li-O-O-Li geometry (Fig. 5 (c)) lying only 60 meV higher. Remarkably, the geometry of this Li-O-O-Li species is very similar to that of bulk Li_2O_2, with O-O distances of $\approx$ 1.50 Å and Li-O distances of 2x1.94 Å and 2x2.05 Å, to be compared with distances in the bulk of 1.55 Å (O-O) and 1.98 Å (Li-O). In this configuration, O_2 is adsorbed on 5c-Mn and the two Li atoms interact with oxygen atoms belonging to the α-MnO_2 surface. We argue that this configuration is the most probable to be the precursor for the formation of Li_2O_2 on the α-MnO_2 (100) surface.

3.5 Implications for Li-air batteries

We now discuss the implications of our results for the functionality of Li-air batteries. First, we notice that, on this surface, molecular adsorption of oxygen is always preferred over dissociative adsorption, both on the bare and on the lithiated surfaces. As a consequence, we expect only the Li-O-O-Li species to form on the (100) surface, and not Li-O-Li. In fact, in previous studies [12,18] it was shown that the formation of Li-O-Li is possible inside the channels of bulk α-MnO_2. It thus seems that Li-O-Li formation is possible only in the bulk but it is unlikely at the surface. This result marks a difference with

β-MnO_2, where dissociative adsorption of oxygen was preferred on the lithiated (110) surface[26]. Our results therefore seem to point out that it might be a characteristic property of α-MnO_2 (100) not to offer to O_2 the possibility to dissociate and subsequently to form Li_2O. This might be the reason behind the better activity and cyclability of a battery with α-MnO_2 as cathode electrocatalyst.

It is important to note that all the formation energies for the Li-O-O-Li molecules that are in the range of $-2.86 \rightarrow -3.23$ eV/Li are more exothermic than the calculated formation energies for the Li_2O_2 molecule (-1.0 eV/Li/O_2) and bulk (-2.60 eV/Li/O_2), using the same computational parameters. We expect therefore the formation of these initial Li-O structures at the α-MnO_2 (100) surface to form easily, to be dissolved with difficulty during battery re-charging, and to offer an advantageous nucleation site for Li_2O_2 formation. On the contrary, on β-MnO_2 it was shown that the formation of Li-O-O-Li species was favored with respect to the formation of Li_2O_2 molecule in the vacuum, but not with respect to bulk Li_2O_2[26]. We expect therefore nucleation of Li_2O_2 on β-MnO_2 to be more difficult than on α-MnO_2 (100). The different behavior on the two catalysts might be related to the superior activity displayed by α-MnO_2 nanowires for the performance for Li-air batteries compared with the β-MnO_2 nanowires[8].

Moreover, on the surface studied here there is a large number of sites where the Li-O-O-Li can form; a large number of nucleation sites might also be important in producing many small Li_2O_2 particles rather than few large ones, with advantages for charge transport and for phase transformation kinetics during charging and discharging. Still, the very exothermic formation energy of the initial Li-O-O-Li species on this surface might imply that these species do not participate in the re-charging, or they do so only at high recharging potentials.

4 Conclusions

The properties of the (100) surface of the manganese oxide α-MnO_2 with a Hollandite structure have been investigated by *ab-initio* methods based on density functional theory (DFT), at the level of DFT+U (U = 1.6 eV). It has been concluded that

(a) The (100) surface has a surface energy comparable to that of (110), and lower than (001); Wulff construction predicts an aspect ratio of approximately 2.1 for nanostructures of this compound.

(b) Molecular oxygen adsorption is preferred over dissociative adsorption at both the bare and lithium-covered α-MnO_2 (100), with adsorption energies between -0.33 eV/O_2 and -0.10 eV/O_2. Molecular adsorption could be a major advantage of this compound over other MnO_2 polymorphs, because it could lead to direct Li_2O_2 formation, avoiding side reactions.

(c) Li adsorption is mostly favored inside the semi-channel at the surface; we expect Li diffusion to be easy along the direction of the semi-channel. The additional charge donated to the surface causes the increase of the magnetic moment of a 5-coordinated Mn (5c-Mn) ions producing an increase of the distance between the 5c-Mn ions and the nearby oxygen atoms.

(d) Co-adsorbing two Li atoms and two oxygen atoms, we find a Li-O-O-Li configuration with a geometry similar to that of bulk Li_2O_2, lying only 60 meV higher than the most stable structures. In this configuration, the oxygen molecule is adsorbed on 5c-Mn and the two adsorbed Li atoms interact also with lattice oxygen.

(e) On (100) there is a high density of sites where the Li-O-O-Li can form, thereby offering a high density of possible nucleation sites for Li_2O_2 formation. This could be of advantage for the kinetics of the process.

5 Acknowledgements

The authors would like to thank Federico Munoz, for fruitful discussions. The YC's position was partly sponsored by the grant "ERC Advanced Grant 320796 – MODPHYSFRICT". Computational resources were provided by CINECA, through the ISCRA-C project AFSGMNO2, and by The Abdus Salam ICTP.

References

1 T. Ogasawara, A. Debart, M. Holzapfel, P. Novak and P. G. Bruce, *J. Am. Chem. Soc.*, 2006, **128**, 1390.
2 P. G. Bruce, S. A. Freunberger, L. J. Hardwick and J. M. Tarascon, *Nat. Mater.*, 2012, **11**, 19.
3 S. A. Freunberger, S. A. Chen, S. A. Peng, J. M. Griffin, L. J. Hardwick, F. Barde, P. Novak and P. G. Bruce, *J. Am. Chem. Soc.*, 2011, **133**, 8040.
4 G. Girishkumar, B. McCloskey, A. C. Luntz, S. Swanson and W. Wilcke, *J. Phys. Chem. Lett.*, 2010, **1**, 2193.
5 P. Albertus, G. Girishkumar, B. McCloskey, R. S. Sanchez-Carrera, B. Kozinsky, J. Christensen and A. C. Luntz, *J. Electrochem. Soc.*, 2011, **158**, A343.
6 M. K. Song, S. Park, F. M. Alamgir, J. Cho and M. Liu, *Mat. Sci. Eng. R: Reports*, 2011, **72**, 203.
7 H. G. Jung, J. Hassoun, J. B. Park, Y. K. Sun and B. Scrosati, *Nat. Chem.*, 2012, **4**, 579.
8 A. Débart, A. Paterson, J. Bao and P. Bruce, *Angew. Chem. Int. Edit.*, 2008, **47**, 4521–4524.
9 M. K. Song, S. Park, F. M. Alamgir, J. Cho and M. Liu, *Mater. Sci. Eng. R: Reports*, 2011, **72**, 203.
10 L. B. Ellis, K. T. Lee and L. F. Nazar, *Chem. Mater.*, 2010, **22**, 691.
11 Y. Shao, S. Park, J. Xiao, J. G. Zhang, Y. Wang and J. Liu, *ACS Catal.*, 2012, **2**, 844.
12 L. Trahey, N. K. Karan, M. K. Y. Chan, J. Lu, Y. Ren, J. Greeley, M. Balasubramanian, A. K. Burrell, L. A. Curtiss and M. M. Thackeray, *Adv. Ener. Mater.*, 2013, **3**, 75–84.
13 C. Wang, L. Sun, Q. Cao, B. Hu, Z. Huang and X. Tang, *Appl. Catal. B: Environ.*, 2011, **101**, 598.

14 X. Tang, J. Li and J. Hao, *Catal. Commun.*, 2010, **11**, 871.
15 V. B. R. Boppana and F. Jiao, *Chem. Commun.*, 2011, **47**, 8973.
16 C. Ling and F. Mizuno, *Chem. Mater.*, 2012, **24**, 3943.
17 E. Cockayne and L. Li, *Chem. Phys. Lett.*, 2012, **544**, 53.
18 D. A. Tompsett and M. S. Islam, *Chem. Mater.*, 2013, **25**, 2515–2526.
19 Y. Crespo, A. Andreanov and N. Seriani, *Phys. Rev. B*, 2013, **88**, 014202.
20 Y. Crespo and N. Seriani, *Phys. Rev. B*, 2013, **88**, 144428.
21 Y. Liu, L. Yu, M. Sun, G. Diao, B. Lan and G. Cheng, *Comput. Theoret. Chem.*, 2014, **1031**, 1 – 6.
22 J. Luo, H. Zhu, F. Zhang, J. Liang, G. Rao, J. Li and Z. Du, *J. Appl. Phys.*, 2009, **105**, 093925–093925.
23 J. Luo, H. Zhu, J. Liang, G. Rao, J. Li and Z. Du, *J. Phys. Chem. C*, 2010, **114**, 8782–8786.
24 B. D. McCloskey, R. Scheffler, A. Speidel, D. S. Bethune, R. M. Shelby and A. C. Luntz, *J. Am. Chem. Soc.*, 2011, **133**, 18038–18041.
25 S. Y. Kang, Y. Mo, S. P. Ong and G. Ceder, *Chem. Mater.*, 2013, **25**, 3328.
26 T. A. Mellan, K. P. Maenetja, P. E. Ngoepe, S. M. Woodley, C. R. A. Catlow and R. Grau-Crespo, *J. Mater. Chem. A*, 2013, **1**, 14879–14887.
27 C. Franchini and R. Podloucky, *Phys. Rev. B*, 2007, **75**, 195128.
28 N. Yamamoto, T. Endo, M. Shimada and T. Takada, *Jpn. J. Appl. Phys*, 1974, **13**, 723.
29 V. I. Anisimov, J. Zaanen and K. O. Andersen, *Phys. Rev. B*, 1991, **44**, 943.
30 A. I. Lichtenstein, V. I. Anisimov and J. Zaanen, *Phys. Rev. B*, 1995, **52**, R5467.
31 P. Giannozzi, S. Baroni, N. Bonini, M. Calandra, R. Car, C. Cavazzoni, D. Ceresoli, G. L. Chiarotti, M. Cococcioni, I. Dabo, A. Dal Corso, S. De Gironcoli, S. Fabris, G. Fratesi, R. Gebauer, U. Gerstmann, C. Gougoussis, A. Kokalj, M. Lazzeri, L. Martin-Samos, N. Marzari, F. Mauri, R. Mazzarello, S. Paolini, A. Pasquarello, L. Paulatto, C. Sbraccia, S. Scandolo, G. Sclauzero, A. P. Seitsonen, A. Smogunov, P. Umari and R. M. Wentzcovitch, *J. Phys.: Condens. Mat.*, 2009, **21**, 395502.
32 S. L. Dudarev, G. A. Botton, S. Y. Savrasov, C. J. Humphreys and A. P. Sutton, *Phys. Rev. B*, 1998, **57**, 1505–1509.
33 M. Cococcioni and S. De Gironcoli, *Phys. Rev. B*, 2005, **71**, 035105.
34 J. P. Perdew, K. Burke and M. Ernzerhof, *Phys. Rev. Lett.*, 1996, **77**, 3865.
35 D. Vanderbilt, *Phys. Rev. B*, 1990, **41**, 7892.
36 H. J. Monkhorst and J. D. Pack, *Phys. Rev. B*, 1976, **13**, 5188–5192.
37 C. Wang, L. Sun, Q. Cao, B. Hu, Z. Huang and X. Tang, *Appl. Catal. B: Environ.*, 2011, **101**, 598 – 605.
38 S. Yamamoto, O. Matsuoka, I. Fukada, Y. Ashida, T. Honda and N. Yamamoto, *J. Catal.*, 1996, **159**, 401 – 409.
39 X. Zhang, X. Sun, H. Zhang, D. Zhang and Y. Ma, *Electrochim. Acta*, 2013, **87**, 637 – 644.
40 M. Xu, L. Kong, W. Zhou and H. Li, *J. Phys. Chem. C*, 2007, **111**, 19141–19147.
41 Y. Chen, C. Liu, F. Li and H.-M. Cheng, *J. Alloy. Compd.*, 2005, **397**, 282 – 285.
42 Y. Chen, C. G. Liu, C. Liu, G. Q. Lu and H. M. Cheng, *Mater. Res. Bull.*, 2007, **42**, 1935 – 1941.
43 G. Wulff, *Z. Kristallogr.*, 1901, **34**, 449.
44 N. Seriani, Z. Jin, W. Pompe and L. C. Ciacchi, *Phys. Rev. B*, 2007, **76**, 155421.
45 N. Seriani and F. Mittendorfer, *J. Phys.: Condens. Mat.*, 2008, **20**, 184023.
46 L. Li, Y. Pan, L. Chen and G. Li, *J. Solid State Chem.*, 2007, **180**, 2896.
47 J. B. Yang, X. D. Zhou, W. J. James, S. K. Malik and C. S. Wang, *Appl. Phys. Lett.*, 2004, **85**, 3160.
48 Y. Lu and Y. Shao-Horn, *J. Phys. Chem. Lett.*, 2013, **4**, 93.
49 M. K. Y. Chan, E. L. Shirley, N. K. Karan, M. Balasubramanian, Y. Ren, J. P. Greeley and T. T. Fister, *J. Phys. Chem. Lett.*, 2011, **2**, 2483.
50 N. Seriani, *Nanotechnology*, 2009, **20**, 445703.
51 T. Bligaard, J. Nørskov, S. Dahl, J. Matthiesen, C. Christensen and J. Sehested, *J. Catal.*, 2004, **224**, 206.
52 I. C. Man, H.-Y. Su, F. Calle-Vallejo, H. H. A, J. I. Martinez, N. G. Inoglu, J. Kitchin, T. F. Jaramillo, J. K. Nørskov and J. Rossmeisl, *ChemCatChem*, 2011, **3**, 1159.
53 R. V. Mom, J. Cheng, M. T. M. Koper and M. Sprik, *J. Phys. Chem. C*, 2014, **118**, 4095.
54 J. Suntivich, k. J. May, H. A. Gasteiger, J. B. Goodenough and Y. Shao-Horn, *Science*, 2011, **334**, 1383.
55 A. Vojvodic and J. K. Nørskov, *Science*, 2011, **334**, 1355.
56 P.-O. Löwdin, *Phys. Rev.*, 1955, **97**, 1474–1489.
57 R. F. W. Bader, *Atoms in Molecules: A Quantum Theory*, Oxford University Press, 1990.
58 N. Seriani, *J. Phys.: Condens. Mat.*, 2010, **22**, 255502.
59 M. M. Branda, N. J. Castellani, R. Grau-Crespo, N. H. de Leeuw, N. C. Hernandez, J. F. Sanz, K. M. Neyman and F. Illas, *J. Chem. Phys.*, 2009, **131**, 094702.